

Article

Analysis of the Flow Behavior and Pressure Fluctuation of a Pump Turbine with Splitter Blades in Part-Load Pump Mode

Wei Xiao ¹, Shaocheng Ren ², Liu Chen ², Bin Yan ¹, Yilin Zhu ³ and Yexiang Xiao ^{3,*} 

¹ Pumped-Storage Technological & Economic Research Institute State Grid Xinyuan Company Ltd., Beijing 100053, China; xiaowei@126.com (W.X.); mxzgyb@163.com (B.Y.)

² China Institute of Water Resources and Hydropower Research, Beijing 100048, China; euler@iwahr.com (S.R.); chenliu@iwahr.com (L.C.)

³ Department of Energy and Power Engineering, Tsinghua University, Beijing 100084, China; zhuy121@mails.tsinghua.edu.cn

* Correspondence: xiaoyex@tsinghua.edu.cn

Abstract: The internal flow of a pump turbine is unstable in part-load pump mode for small guide-vane openings, and the strong vibration caused by pressure pulsation is related to the safe and stable operation of the unit. A pump turbine with a six-splitter-blade runner was chosen for unsteady simulation analyses. A standard k-epsilon turbulence model was adopted to study the unsteady flow and pressure pulsation in part-load pump mode. The predicted results show that the flow in the draft tube and the runner with splitter blades was relatively stable and the flow of the blade-to-blade channel was symmetrical. When the inlet and outlet velocity distribution of the vanes was not uniform, a vortex began to form in the stay-vane domain. The reason for this vortex formation is explained, and it is pointed out that the existence of the vortex and backflow leads to uneven velocity distribution. The unsteady calculation results showed that the pressure-pulsation peak-to-peak amplitudes in the vaneless area and guide vanes were much higher than those of other monitor points because of rotor–stator interference between the rotating runner and the vanes. In addition, the pulsation characteristics of the monitor points at different circumferential positions in the vaneless region were quite different. In the vaneless area, the velocity gradient along the circumferential direction was very large, and there was a phenomenon of backflow. Also, the pressure pulsation was 0.2 times that of the runner rotational frequency, and the blade-passing frequency was a third-order frequency. At the outlet of the guide vane, the pressure pulsation was mainly of a low frequency with a complex vortex flow. Finally, the pressure pulsation began to decrease rapidly in the stay-vane region.

Keywords: pump turbine; splitter blades; pressure pulsation; part-load pump mode; numerical simulation



Citation: Xiao, W.; Ren, S.; Chen, L.; Yan, B.; Zhu, Y.; Xiao, Y. Analysis of the Flow Behavior and Pressure Fluctuation of a Pump Turbine with Splitter Blades in Part-Load Pump Mode. *Energies* **2024**, *17*, 2402. <https://doi.org/10.3390/en17102402>

Academic Editor: Massimiliano Renzi

Received: 9 April 2024
Revised: 8 May 2024
Accepted: 10 May 2024
Published: 16 May 2024



Copyright: © 2024 by the authors. Licensee MDPI, Basel, Switzerland. This article is an open access article distributed under the terms and conditions of the Creative Commons Attribution (CC BY) license (<https://creativecommons.org/licenses/by/4.0/>).

1. Introduction

In September 2020, China made a solemn commitment to the world to reach a carbon peak by 2030 and carbon neutrality by 2060 [1]. Pumped storage power stations, clean energy, can effectively reduce carbon emissions [2]. A pumped storage power station is a very-large-capacity energy storage site [3], and its ability to regulate and stabilize the power grid plays a crucial role in new types of solar–wind–water complementary power systems [4–6]. At present, many pumped storage power stations are undergoing or have carried out the modification of splitter blades [7,8], so research on the performance of pump-turbine runners with splitter blades is of great practical significance.

Recently, more research has been focused on the design of splitter blades and the flow characteristics and pressure pulsation of pump turbines. Song et al. [9] compared the performances of runners with different splitter-blade numbers via simulation, and pointed out that two-thirds is the optimal proportion of the diameter of the long-blade skeleton line to the short-blade skeleton line. On this basis, Hu [10,11] explored the

influence of various design parameters on the performance and S-characteristics of a pump turbine with splitter blades. Researchers [12–15] believe that the pressure pulsation–dominant frequency component is the key factor causing vibration in units and factory buildings, and vibration has an effect on the variation in the pressure amplitude–frequency spectrum [16]. Therefore, many scholars [17–19] have conducted studies on pressure-pulsation characteristics in various transition processes and summarized the relationship between the pressure load in the vaneless area and the pulsation amplitude. Wang [20] and Xu [21] analyzed the attenuation law of high- and low-frequency spreading upstream and downstream in the vaneless area, and elucidated the frequency composition and causes of pressure pulsation in the vaneless area. Le et al. [22] explained that an abnormal change in pressure-pulsation amplitude near the monitoring point of a guide vane driven by a small-opening pump turbine is related to the flow pattern. Zhao et al. [23] conducted a numerical simulation of a pump turbine with an off-design pump, and found that the flow in the runner channel was asymmetrical with obvious flow separation and vortices. They pointed out that this asymmetry was related to the asymmetric pressure pulsation in the channel. Kassanos et al. [24,25] pointed out that splitter blades can improve the performance of pump turbines and reduce pressure pulsation under small-load conditions. Gui et al. [24] simulated the performance of splitter-blade pump turbines with the same opening and different heads, and verified it with laser Doppler velocimetry (LDV). Finally, they used the entropy generation theory to analyze the source of the loss, and pointed out that the hydraulic loss in the flow channel was mainly affected by the velocity gradient, not by the vortex structure. Many scholars [25–27] have studied the S-characteristic region through numerical calculations or PIV tests, obtained the flow and pressure-pulsation conditions at different working points, analyzed the positions of and reasons for vortex generation, and found that the flow under pump-braking conditions was the most unstable. In order to improve the S-characteristics of pump turbines from a design point of view, researchers [28–30] have established the correlations between various geometric parameters of pump turbines and S-characteristics, and improved the S-characteristics by changing the geometric dimensions.

Based on the part-load pump mode with a small guide-vane opening of a pump turbine with six splitter blades, this paper analyzes flow behavior and pressure pulsation numerically, and the cause of vortex generation and the relationship between intense pulsation and the vortex is explained.

2. Numerical Model and Mathematical Model

2.1. Computational Model and Simulation Domain

The model of the pump turbine with 6 splitter blades was based on a prototype pumped storage unit. The prototype runner diameter was 3.89 m with 12 blades, 20 guide vanes, and 20 stay vanes. The turbine's rated speed was 500 rpm. The flow channel of the splitter-blade model unit included the volute, guide vanes, stay vanes, and draft tube. The overall 3D flow channel is shown in Figure 1.

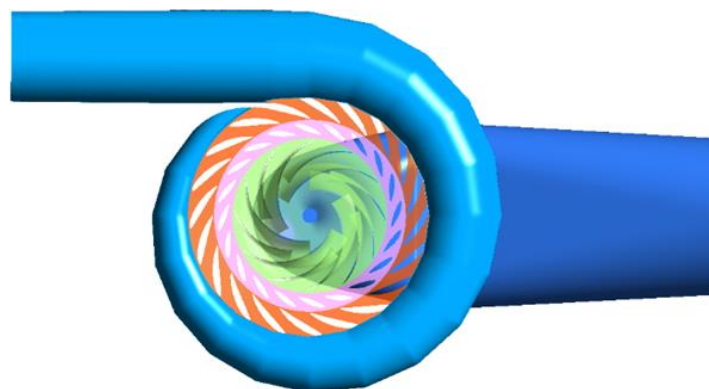


Figure 1. The entire flow domain of the pump turbine with splitter blades.

When operating in pump mode, the optimal opening is about 19° . To study the model performance's deviation from the optimal operating conditions, the part-load operation condition with an opening of 12° was selected. The runner rated speed was 500 rpm during the numerical simulation. According to the model test, the flow rate was an approximately 70% rated load with the guide-vane opening of 12° .

2.2. Mesh and Boundary Conditions

The overall flow channel of the turbine was divided, wherein an unstructured grid was used for the volute, and a structured grid was used for the draft tube, guide vane, stay vane, and runner blade. After the grid independence verification, in total, 5.48 million cells were finally determined, including 1.49 million cells for the volute, 1.12 million cells for the guide vanes, 0.92 million cells for the stay vanes, 1.56 million cells for the runner blade, and 0.39 million cells for the draft tube, as shown in Figure 2.

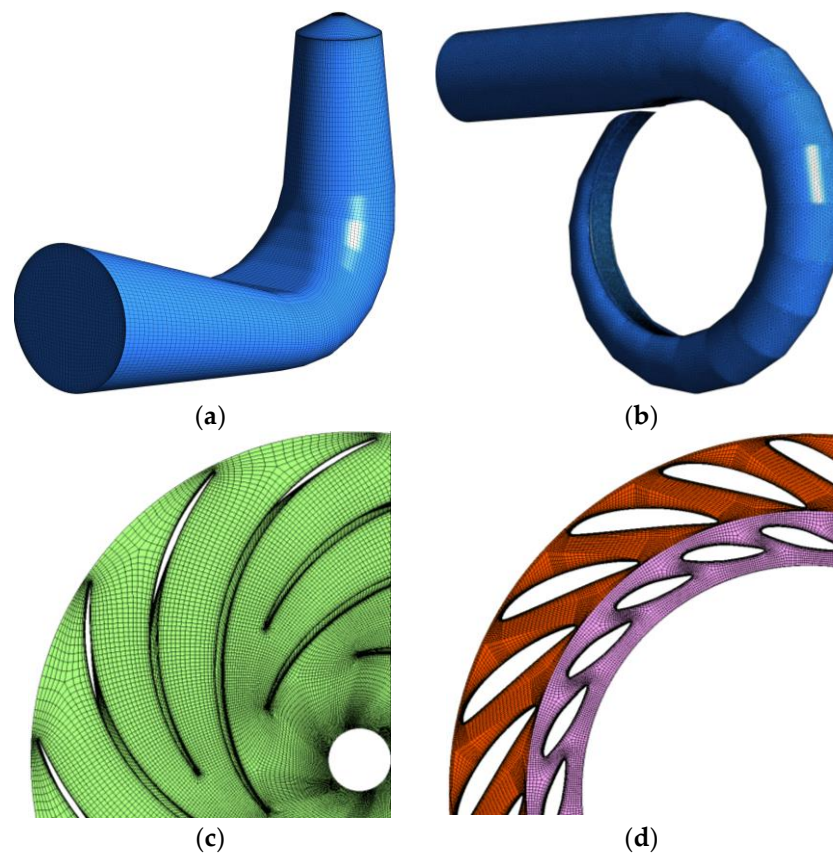


Figure 2. Mesh of the pump turbine with the splitter-blade runner: (a) draft tube, (b) volute, (c) runner, (d) vanes.

The initial condition in the unsteady calculation used the full flow-channel data after the convergence of the steady calculation. The inlet boundary adopted the mass flow inlet condition, and the outlet boundary condition was set as the local atmospheric pressure. The wall was set as a non-slip boundary condition. A slip mesh model was used at the interface to simulate the unsteady flow field.

The control equation used the continuous equation of incompressible fluid and the Reynolds-averaged Navier–Stokes equation to simulate the water flow in the turbine, and the standard k-epsilon turbulence model was used to solve the unsteady flow, so it was necessary to ensure that the y^+ of the grid near the wall was about 30–100. The effects of undissolved gases and cavitation were not considered. The time step of unsteady calculation was 0.0012 s, which is 1/100 of the runner rotation period. The data were saved for each calculation step. To correctly predict the irregular behavior in the overall

flow channel, an unsteady calculation of the physical time of about 2.4 s was performed at this working condition, and the last 1.2 s of the calculation time was used for the data processing and analyses.

2.3. Arrangement of Monitor Points

The monitor points were set to monitor the pressure pulsation of each component for unsteady calculation. The distribution of rotating monitor points in the runner is shown in Figure 3a. The six long blades were named R1–R6 counterclockwise, and the monitor points RP1A–RP1H were set in the channel on the pressure side of the long blade R1, and the monitor points RS1A–RS1H were set in the section side of the long blade R1. The monitor point positions in the middle of the channel were named with the same naming rules used for the other parts.

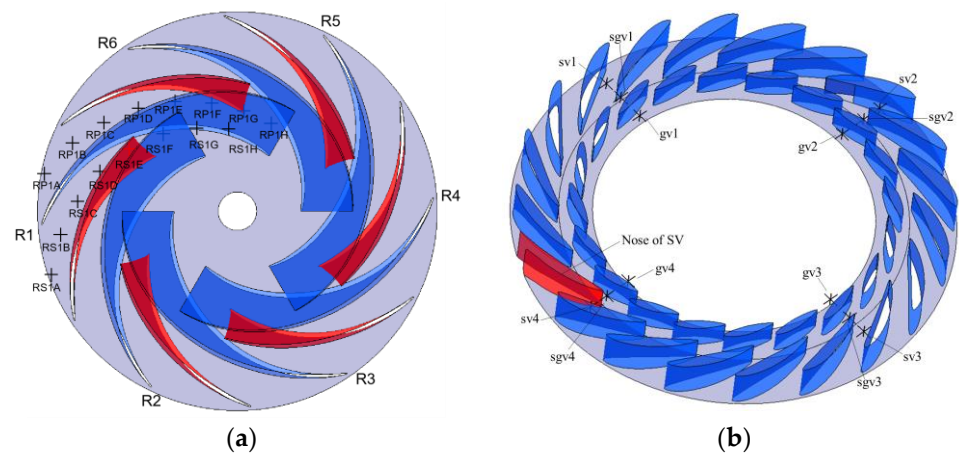


Figure 3. Distribution of the monitor points: (a) monitor points in the runner, (b) monitor points in the vanes.

In Figure 3b, the gv monitoring points are located in the vaneless area between the guide vanes and the runner; gv1–gv4 are the monitoring points on the middle span of the vaneless area between the rotating runner and guide vanes, sgv1–sgv4 are the monitoring points between the guide vanes and stay vanes, and sv1–sv4 are the monitoring points located in the middle span of stay vanes. These monitor points were fixed in the same positions for the unsteady calculations.

3. Results and Discussions

3.1. Comparison of Hydraulic Performance and Flow Behavior in Pump Mode

Figure 4 shows the hydraulic efficiency results of the test and simulation under different guide-vane openings in pump mode. The efficiency reaches the highest at a guide-vane opening of about 19° . After deviating from the optimal opening, the hydraulic efficiency decreases. The error between the prediction and the test is small under the small guide-vane opening, and the error gradually increases with the increase in the guide-vane opening. The efficiency in the numerical predictions is lower than the experimental value. Although there is a certain deviation in the hydraulic efficiency results, the trend of the numerical simulation and experimental results is generally consistent, which verifies the accuracy and reliability of the three-dimensional simulation method used in this paper.

Figure 5 shows the velocity distribution of the various components of the pump turbine when the guide-vane opening is 12° . Figure 5a is the velocity diagram for the draft tube. The draft tube is used as a suction pipe in the pump condition, and the overall flow is stable without flow separation and vortexes. Figure 5b is the velocity diagram for the volute. The velocity distribution of the volute inlet close to the runner is uneven along the circumferential direction. The mass flow average velocity of the volute inlet in the pump

condition is 26.97 m/s. Except some obvious velocities in Figure 5b being higher than 40 m/s, the velocity in the volute is less than 20 m/s.

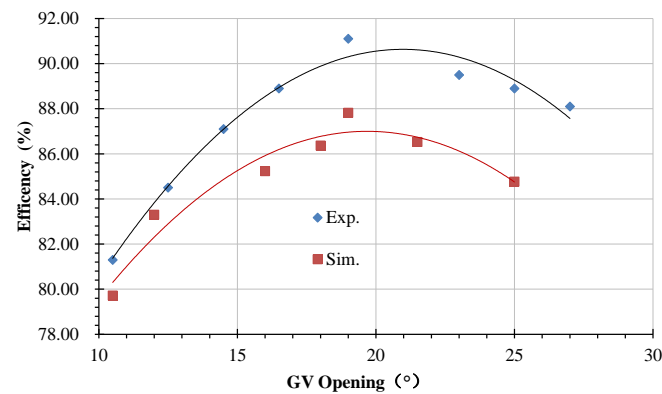


Figure 4. Pump-mode hydraulic efficiency under different openings.

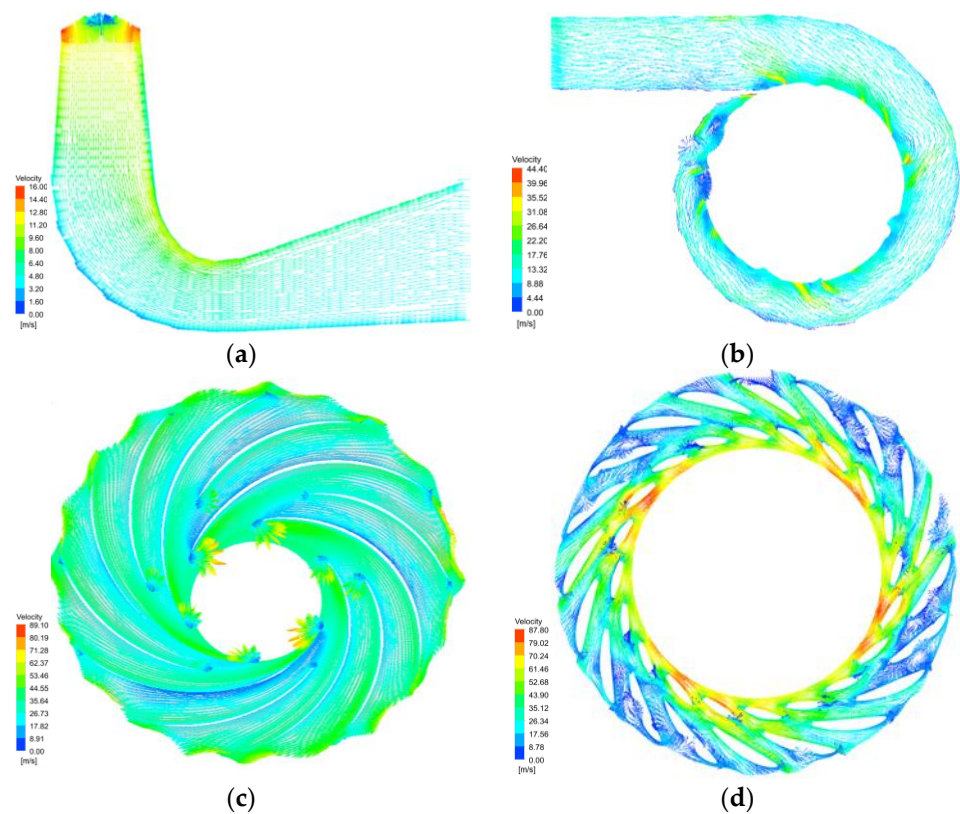


Figure 5. Velocity vector in the pump turbine's entire flow passage: (a) draft-tube velocity, (b) volute velocity, (c) 0.5-span turbo surface velocity, (d) vane velocity.

The uneven distribution of volute velocity is related to the vortex in the stay vanes in Figure 5d. Due to the small guide-vane opening, the fluid velocity in the outlet of the guide vanes is too large along the circumferential direction. The flow angle of the guide-vane outlet does not match the inlet angle of the stay vanes, so flow separation and vortices occur. The area where the vortices are generated blocks the flow, which manifests in a too-small velocity. Since the vortex blocks the flow, some of the fluid that should enter the corresponding stay-vane channel will partially enter the other stay-vane channels. So, there are several significant velocities above 40 m/s in Figure 5d.

Figure 5c is the velocity diagram of the runner-blade channel, where the flow in a group of splitter-blade channels is uniform and the velocity gradient is relatively gentle

without the vortex and reflux. However, the long-blade pressure-side velocity is obviously lower than that of the short blade, which indicates that the velocity distribution of the runner inlet is uneven. This means that the flow rate distribution is also uneven. The flow rate of the long-blade pressure side will be less than that of the short-blade pressure side. According to the Bernoulli equation, the pressure of the long-blade pressure side is significantly higher than that of the short-blade pressure side.

In Figure 5d, the velocity is uneven and the flow is disordered. Figure 6 shows the velocity distribution along the circumference direction of the guide-vane inlet and outlet. The inlet of the guide vane, that is, the vaneless area between the runner and the guide vane, is seriously influenced by the rotor–stator interaction. Along the circumferential direction, the velocity gradient of the inlet velocity's tangential component is large, distributed from 10 m/s to 80 m/s. The inlet velocity radial component mainly fluctuates from 0 to 20 m/s. The radial velocities somewhere are less than 0, indicating that some fluid flows back to the runner. This reflux is also the reason for the uneven distribution of the tangential velocity. The velocity gradient of the guide-vane outlet tangential velocity is also large, distributed from 0 to 70 m/s. The radial component of the outlet velocity mainly fluctuates from 0 to 40 m/s. Also, the radial velocities somewhere are less than 0, indicating that some fluid flows back to the guide vane. In summary, the non-uniform distribution of the guide-vane inlet and outlet velocity along the circumference is due to the vortex and reflux. The vortex and reflux are caused by the mismatch at the small opening between the flow direction and the inlet angle of the guide vane.

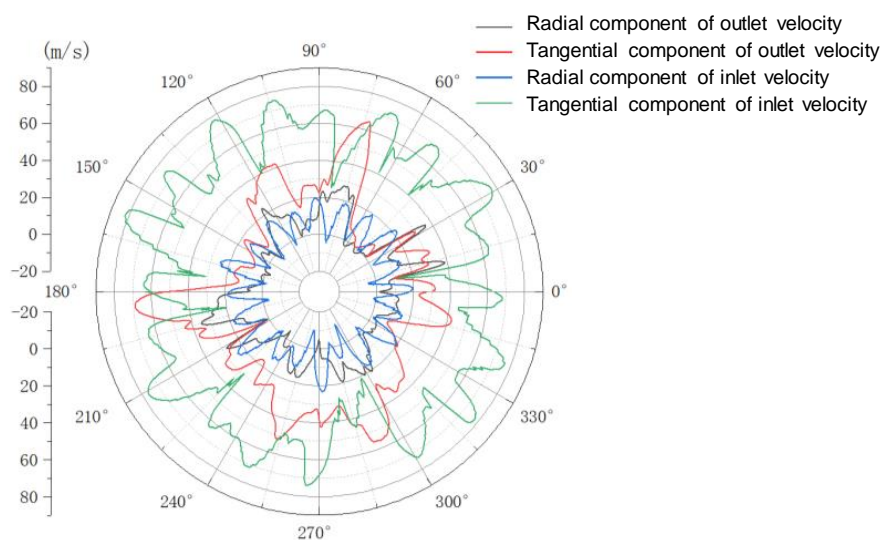


Figure 6. Velocity distribution along the runner's guide-vane and stay-vane circumference.

3.2. Unsteady Flow Characteristics in the Runner and Guide Vanes

Figure 7 displays the velocity streamline on the 0.5-span surface of the runner and vanes under small-opening conditions in the pump mode, in which Figure 7a–f represent the variation in the streamline within the runner and vanes during one round of runner rotation. The streamline distribution in the runner blade was uniform and the flow was in good condition. The velocity along the long-blade pressure side was always slightly lower than that of the short-blade pressure side, and was in good agreement with the result obtained from the steady simulation. The velocity in the vaneless zone between the runner and the guide vanes was generally greater than that of the other positions. The velocity distribution in the vaneless zone along the circumferential direction was not uniform, while no obvious variation in velocity showed up in the same region at each moment.

The flow behavior in the guide vanes was much more complex. A plurality of obvious vortices was produced as the runner rotated for one round. The positions of the vortices almost remained the same as they formed and dissipated. Because of the existence of

the vortices, in the pump mode of the pump turbine, the fluid flowing out of the guide vanes was blocked by the vortices when entering some of the stay-vane channels. This phenomenon also existed when the fluid entered the guide vanes from the runner. If there were vortices blocked in a certain flow channel, the fluid would enter either the former or the latter flow channel. The tangential velocity of the fluid entering the former channel would decrease, while the tangential velocity entering the latter channel would increase.

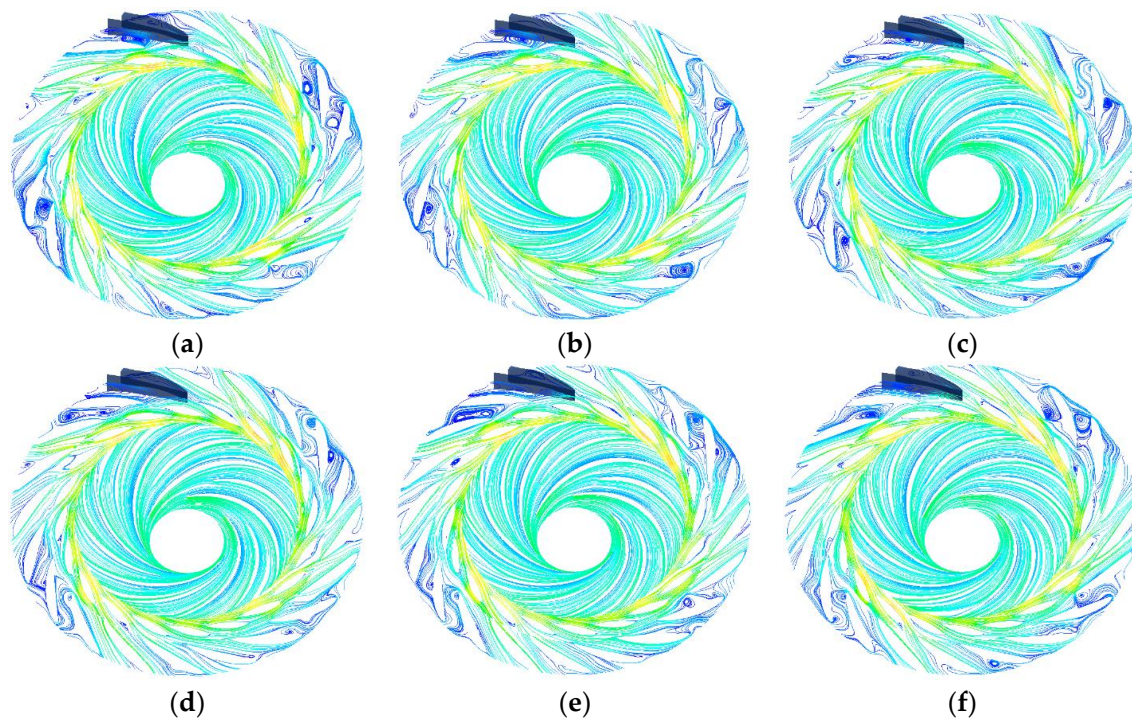


Figure 7. Variation in streamlines during rotation for one rotation cycle: (a) 0 T, (b) 1/6 T, (c) 2/6 T, (d) 3/6 T, (e) 4/6 T, (f) 5/6 T.

3.3. Analysis of Pressure-Pulsation Characteristics at the Measuring Points

Due to the periodicity of the runner, taking the middle R1 blade as an example, RP1 and RS1 are a set of splitter-blade channels, and the specific position of each measuring point is shown in Figure 3a. Figure 8 shows the relative peak-to-peak pressure fluctuation amplitude of the measuring points in the runner channel. Comparing the peak-to-peak value changes for the two groups of channels, from point H to A, in the flow direction of the pump mode, it gradually approaches the vaneless area, and the influence of the rotor–stator interference becomes more serious. The peak-to-peak pressure fluctuation of the two channels increases. The peak-to-peak values of the RP1 and RS1 channels near the vaneless region are not significantly different. When away from the vaneless region, the peak-to-peak value of the RP1 channel is slightly larger than that of the RS1 channel.

The motion of the turbine runner has the property of periodicity. We take the runner blade of R1 as an example, while the specific location of this measuring point is shown in Figure 3a. Figure 9 shows the pressure-pulsation spectrum analysis on measuring points in the runner-blade channel, in which Figure 9a,b display the pressure-pulsation spectrum in different channels. The rotation frequency is named f_n . For example, $20 f/f_n$ represents 20 times the rotation frequency. Due to the splitter blades having two types of blade, there are also two types of flow channels. RP1 is the flow channel on the pressure side of the long blade R1, while RS1 is the flow channel on the suction side of the long blade R1.

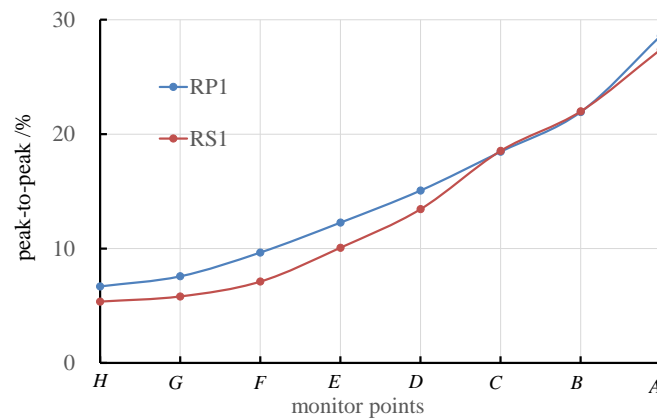


Figure 8. The relative peak-to-peak pressure amplitude on the runner.

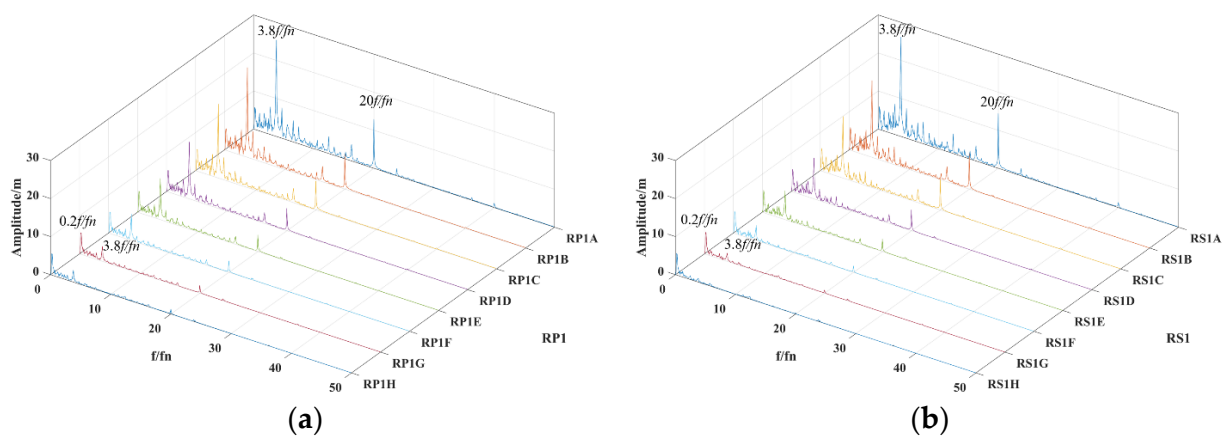


Figure 9. Spectrum analysis of the runner-blade monitoring-point pressure pulsation: (a) RP1 pressure-side flow channel, (b) RS1 suction-side flow channel.

By comparing the pressure pulsation of RP1 and RS1 in Figure 9, we find that the same frequency distribution pattern occurred in both flow channels, and the difference in pulsation amplitude was also insignificant. It can be considered that the pressure pulsation of long and short blades under the pump condition shared the same variation pattern.

The monitor points RP1A and RS1A were close to the vaneless zone, so they were most affected by the rotor–stator interference. The farther the measuring points from the vaneless zone, the lower the amplitude of the pressure fluctuation. Meanwhile, the dominant frequency and secondary frequency also varied. The dominant frequency and secondary frequency of the measuring points near the vaneless zone were $3.8 f/fn$ and $20 f/fn$, respectively. The dominant frequency and secondary frequency of the measuring points in the runner flow channel close to the draft tube were $0.2 f/fn$ and $3.8 f/fn$, respectively.

By observing the variation trend of the dominant frequency in the splitter-blade channel, from the monitor points RP1A to RP1H, it was found that as the points gradually moved away from the vaneless zone and guide vanes, the dominant frequency of $3.8 f/fn$ for RP1A, as well as the non-integer multiple frequency near the dominant frequency, gradually declined or even disappeared. This result showed that the non-integer multiple frequency was affected by the vaneless zone. The secondary frequency $20 f/fn$ was affected by the number of guide vanes. The influence of the rotor–stator interference was continuously weakened as the measuring points gradually moved away from the guide vane, and the amplitude of the pressure pulsation became lower. The low-frequency amplitude of $0.2 f/fn$ remained unchanged and gradually became the dominant frequency.

Figure 10 shows the peak-to-peak pressure-pulsation amplitude at the measuring points in the guide-vane area, and Positions 1, 2, 3, and 4 correspond to the positions of the runner with an interval of 90° on one circle. The gv monitor point represents the

vaneless area. Due to the influence of rotor–stator interaction, the pressure pulsation near the vaneless area is obviously the most intense. The amplitude of the pressure pulsation gradually increases from RPH at the runner inlet to RPA at the runner outlet. From RPA at the runner outlet to gv at the vaneless area, to sgv between the stay vanes and the guide vanes, the peak-to-peak values of pressure pulsation are always very high. From sgv to the sv area inside the stay vanes, the peak-to-peak amplitude of the pressure pulsation begins to decrease significantly.

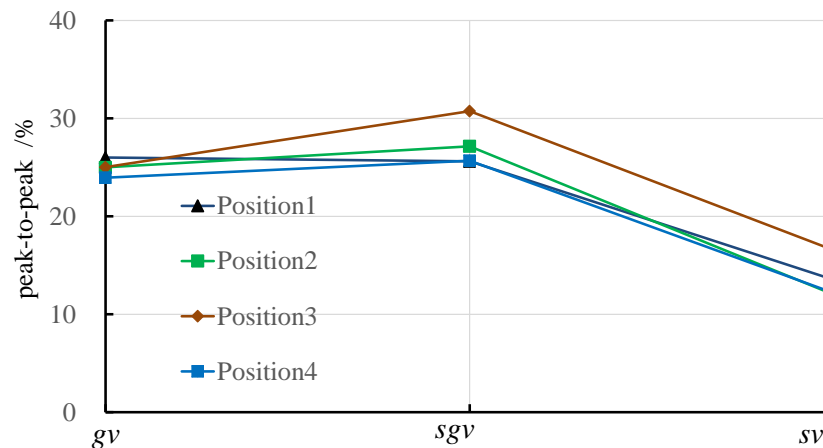


Figure 10. Peak-to-peak amplitude around the vanes.

In order to analyze the causes of pressure pulsation in the vaneless area, two monitor points of gv2 in the vaneless area and sgv2 in the middle position of the stay vanes and the guide vanes are taken as examples for analysis. According to the time-domain signal analysis, the overall trend of the pressure changes at the gv2 monitor point and the sgv2 monitor point is the same, in the range of 1.2 s to 2.4 s, within which 0.12 s is the time taken for the runner to rotate one cycle. The number and intensity of oscillations at the gv2 monitor point in any time period are greater than those at the sgv2 monitor point. As shown in the time-domain diagram, the curve of the gv2 pressure changing with time is not smooth, while the curve of sgv2 is smooth. The reason for this is that gv2 is a monitor point in the vaneless area, which is closer to the runner blade and is greatly affected by the rotor–stator interaction.

The frequency-domain diagram in Figure 11 shows the first five orders of frequency of the pressure pulsation and the amplitude corresponding to each frequency. The first three frequencies of the gv2 monitor point are $0.2 f/fn$, $0.4 f/fn$, and $12 f/fn$, and the first three frequencies of the sgv2 monitor point are $0.4 f/fn$, $0.2 f/fn$, and $0.6 f/fn$. The monitor point gv2 is closer to the runner blade, which is affected by the rotor–stator interaction. This leads to the observation that in the frequency-domain diagram, the blade-passing frequency (referred to as the rotational frequency) of $12 f/fn$ appears in the first five frequencies. Under normal conditions, the blade’s value of rotational frequency is the main frequency of the pressure pulsation in the vaneless area, but in the case of small-opening pump conditions, the vaneless area is more affected by the low frequencies, mainly $0.2 f/fn$ and $0.4 f/fn$. The sgv2 monitor point is far away from the runner, which is less affected by the rotational frequency, and is mainly affected by the low frequencies, too. The amplitude of $0.2 f/fn$ at the gv2 point is relatively larger, indicating that it is generated in the vaneless area and transmitted downstream. The amplitude of $0.4 f/fn$ at the sgv2 monitor point is relatively larger, indicating that this amplitude is generated near the stay vanes and transmitted to the upstream vaneless area. It is speculated that this is related to the vortex generated at the stay vanes in Figure 7. In Figure 11, the $0.2 f/fn$ amplitude in the runner-blade channel still exists near the draft tube, indicating that this amplitude is also generated in the vaneless area and transmitted upstream, and the low-frequency amplitude of $0.2 f/fn$ is hardly attenuated during this transmission to the upstream runner.

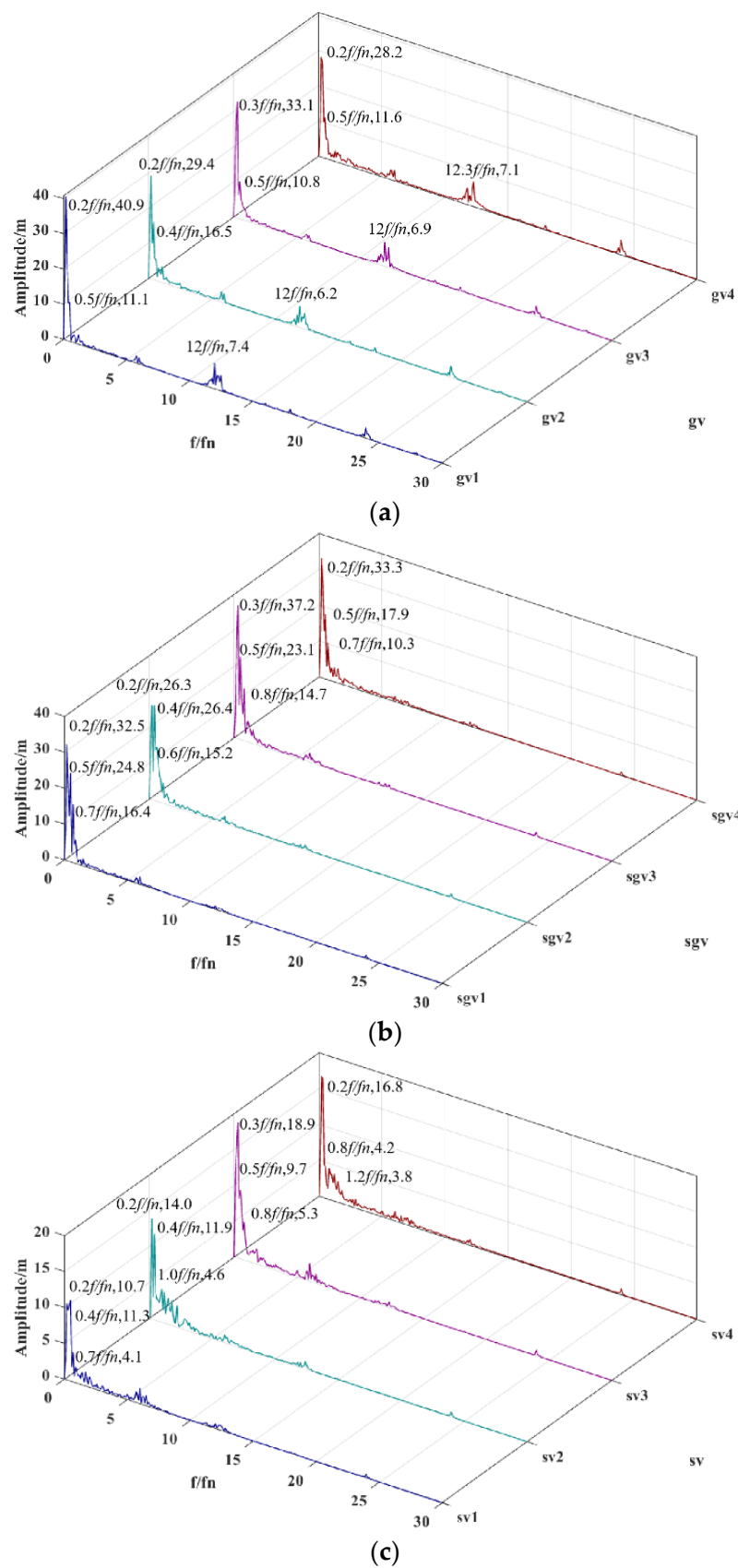


Figure 11. Spectrum analysis of the pressure pulsation around the vanes: (a) monitoring point gv in the vaneless area; (b) monitoring point sgv between the stay vane and guide vane; (c) monitoring point sv on the stay vane.

4. Conclusions

An unsteady numerical analysis was carried out under 12° small-opening conditions in pump mode for a pump turbine with splitter blades. In this paper, the flow characteristics of the runner-blade channel, as well as the pressure pulsation of the entire flow passage at various monitoring points, are analyzed. The conclusions are drawn as follows.

Under the pump mode with a small opening, the flow is relatively stable in the draft tube and runner-blade channels, while, due to vortex generation and backflow, the velocity distribution in the guide-vane region is not circumferentially uniform. The vortex and backflow in the guide vanes are induced by the mismatch between the guide-vane inlet angle and the flow direction. And the downstream flow in the stay vanes and volute is also very complex.

The peak-to-peak pressure amplitude in the vaneless zone, as well as at the guide-vane monitor points, was larger than that of the others. The dominant frequency of the pressure fluctuation in the vaneless zone was not the rotational frequency but the low frequency caused by the vortex at the guide vanes. Meanwhile, the pressure pulsation at the measuring points in the vaneless zone was also greatly affected by rotor–stator interference, which manifested in the appearance of the runner rotational frequency and its multiplication. By comparing the pressure pulsation at two sorts of measuring points in the splitter-blade flow channels, the results show that in the pump mode, the pressure-pulsation frequency distribution between the different runner splitter-blade channels was the same. The closer a measuring point was to the vaneless zone, the greater the influence of rotor–stator interference there would be, which manifested in the amplitude increasing by 20 f/n . If it was closer to the draft tube, the low frequency of 0.2 f/n would gradually become the dominant frequency.

Author Contributions: W.X. conceived the idea and the study design; S.R. conceived the idea and took part in the study design and supervision; L.C. performed the simulations and prepared the manuscript; B.Y., Y.Z. and Y.X. carried out the literature review and the writing. All authors have read and agreed to the published version of the manuscript.

Funding: This work was supported by the State Grid Xinyuan Company LTD Science and Technology Project (No. SGXYKJ-2022-043).

Data Availability Statement: Data are contained within the article.

Conflicts of Interest: Authors Wei Xiao and Bin Yan were employed by the company Pumped-Storage Technological & Economic Research Institute State Grid Xinyuan Company Ltd. The remaining authors declare that the research was conducted in the absence of any commercial or financial relationships that could be construed as a potential conflict of interest.

References

1. You, L.; Fan, Y. Design and research of multi-energy complementary power generation system based on pumped storage under the goal of carbon emission peak and carbon neutrality. *Hydropower Pumped Storage* **2021**, *7*, 40–44. (In Chinese)
2. Li, J.; Zhao, Z.; Xu, D.; Li, P.; Liu, Y.; Mahmud, M.A.; Chen, D. The potential assessment of pump hydro energy storage to reduce renewable curtailment and CO₂ emissions in Northwest China. *Renew. Energy* **2023**, *212*, 82–96. [[CrossRef](#)]
3. Kan, K.; Binama, M.; Chen, H.; Zheng, Y.; Zhou, D.; Su, W.; Muhirwa, A. Pump as turbine cavitation performance for both conventional and reverse operating modes: A review. *Renew. Sustain. Energy Rev.* **2022**, *168*, 112786. [[CrossRef](#)]
4. Wang, X.; Virguez, E.; Xiao, W.; Mei, Y.; Patiño-Echeverri, D.; Wang, H. Clustering and dispatching hydro, wind, and photovoltaic power resources with multiobjective optimization of power generation fluctuations: A case study in southwestern China. *Energy* **2019**, *189*, 116250. [[CrossRef](#)]
5. Jiang, G.; Peng, Y.; Ji, C.; Luo, S.; Yu, X. Hydro-wind-solar power complementary short-term optimal scheduling considering participation of price-based demand response. *J. Hydroelectr. Eng.* **2023**, *42*, 1–12. (In Chinese)
6. Ruppert, L.; Schürhuber, R.; List, B.; Lechner, A.; Bauer, C. An analysis of different pumped storage schemes from a technological and economic perspective. *Energy* **2017**, *141*, 368–379. [[CrossRef](#)]
7. Liu, P.; Yang, H.; Ma, Y.; Zheng, J.; Fan, J. Calculation and experimental study on the transition process before and after the modification of unit 4 of Heimifeng pumped storage power station. *Hydropower Pumped Storage* **2023**, *9*, 85–91. (In Chinese)
8. Zheng, J.; Liu, P.; Liang, Q.; Ren, S.; Zeng, Y. Review of localization and hydraulic optimization for heimifeng pumped storage units. *Hydropower Pumped Storage* **2023**, *9*, 87–98. (In Chinese)

9. Song, X.F.; Mao, X.L.; Lu, J.H.; Zhang, X. CFD-based optimal design of pump-turbine runner with long and short blades. *Water Resour. Hydropower Eng.* **2021**, *52*, 115–123. (In Chinese)
10. Hu, J.; Zhao, Z.; He, X.; Zeng, W.; Yang, J.; Yang, J. Design techniques for improving energy performance and S-shaped characteristics of a pump-turbine with splitter blades. *Renew. Energy* **2023**, *212*, 333–349. [[CrossRef](#)]
11. Hu, J.; Yang, J.; Zeng, W.; Yang, J. Effect of the Speed Factor on the Amplitude of the Blade Passing Frequency in the Vaneless Space of a Pump Turbine in Turbine Mode. *J. Fluids Eng. Trans. ASME* **2021**, *143*, 111203. [[CrossRef](#)]
12. Zhang, L.; Li, J. Characteristic analysis of pressure fluctuation in the non-blade area of a pump-turbine under turbine Condition. *Large Electr. Mach. Hydraul. Turbine* **2017**, *1*, 60–63. (In Chinese)
13. Yuan, S.; Fang, Y.; Yuan, J.; Zhang, J. Review on vibration problems of power units in commissioned pumped storage projects in China. *J. Hydroelectr. Eng.* **2015**, *34*, 1–15. (In Chinese)
14. Tian, Z. Key technology development of high head pump turbine. *Hydropower Pumped Storage* **2017**, *3*, 39–45, 54. (In Chinese)
15. Zhao, Y.; Zhang, F.; Chen, S.; Xu, Y. Amplitude Characteristic of Vaneless Zone Pressure in Load Rejection Process for Pumped-Storage Units. *Yellow River* **2023**, *45*, 134–139. (In Chinese)
16. Stosiak, M.; Karpenko, M.; Deptuła, A.; Urbanowicz, K.; Skačkauskas, P.; Deptuła, A.M.; Danilevičius, A.; Šukevičius, Š.; Łapka, M. Research of vibration effects on a hydraulic valve in the pressure pulsation spectrum analysis. *J. Mar. Sci. Eng.* **2023**, *11*, 301. [[CrossRef](#)]
17. Trivedi, C.; Cervantes, M.J.; Gandhi, B.K.; Dahlhaug, O.G. Transient Pressure Measurements on a High Head Model Francis Turbine During Emergency Shutdown, Total Load Rejection, and Runaway. *J. Fluids Eng.* **2014**, *136*, 121107. [[CrossRef](#)]
18. Yin, C.; Zeng, W.; Yang, J. Transient simulation and analysis of the simultaneous load rejection process in pumped storage power stations using a 1-D-3-D coupling method. *J. Hydrodyn.* **2021**, *33*, 979–991. [[CrossRef](#)]
19. Lu, J.; Qian, Z.; Lee, Y.H. Numerical investigation of unsteady characteristics of a pump turbine under runaway condition. *Renew. Energy* **2021**, *169*, 905–924. [[CrossRef](#)]
20. Liu, T.; Li, C.; Liu, J.; Wang, Y. Analysis of pressure fluctuation characteristics of pump-turbine under pump operating conditions. *Hydropower Northeast China* **2023**, *41*, 68–70. (In Chinese)
21. Xu, H.; Lu, L.; Wang, W.; Zhao, L. Study on generating mechanism of pressure fluctuation in the vaneless region of the pump-turbine. *J. China Inst. Water Resour. Hydropower Res.* **2020**, *18*, 248–256. (In Chinese)
22. Le, Z.; Xiao, Y.; Gui, Z.; Zeng, C.; Zhu, W. Unsteady flow and pressure pulse analysis of a Francis pump-turbine on reverse pump zone with small guide vane opening. *J. Hydraul. Eng.* **2018**, *49*, 1541–1549. (In Chinese)
23. Zhao, X.; Xiao, Y.; Wang, Z.; Wang, Z.; Luo, H.; Ahn, S.-H.; Yao, Y.; Fan, H. Numerical analysis of non-axisymmetric flow characteristic for a pump-turbine impeller at pump off-design condition. *Renew. Energy* **2018**, *115*, 1075–1085.
24. Kassanos, I.; Chrysovergis, M.; Anagnostopoulos, J.; Papantonis, D.; Charalampopoulos, G. Numerical Performance Evaluation of Design Modifications on a Centrifugal Pump Impeller Running in Reverse Mode. *AIP Conf. Proc.* **2016**, *1738*, 480084.
25. Kassanos, I.; Anagnostopoulos, J.; Papantonis, D. Numerical investigation of draft tube pressure pulsations in a Francis turbine with splitter blades. *J. Phys. Conf. Ser.* **2017**, *813*, 012049. [[CrossRef](#)]
26. Gui, Z.; Xu, Z.; Li, D.; Zhang, F.; Zhao, Y.; Xu, L.; Zheng, Y.; Kan, K. Analysis of the Energy Loss Mechanism of Pump-Turbines with Splitter Blades under Different Characteristic Heads. *Water* **2023**, *15*, 2776. [[CrossRef](#)]
27. Zhu, W.; Xiao, Y.; Yao, Y.; Luo, Y. Internal flow behaviour analysis of Francis pump-turbine in S-curve region with small guide vane opening. *J. Hydroelectr. Eng.* **2015**, *34*, 138–144. (In Chinese)
28. Wang, L.; Liao, W.; Lu, J.; Zhao, Y.; Ruan, H.; Wang, J. Pressure fluctuations in pump turbines in S zone based on weakly compressible modeling. *J. Hydroelectr. Eng.* **2017**, *36*, 69–78. (In Chinese)
29. Xu, L.; Liu, D.; Li, Z.; Zhao, X.; Liu, X. Experimental and numerical simulation research on flow characteristics of model pump-turbine in four-quadrant operating quadrants. *J. Energy Storage* **2022**, *54*, 105083. [[CrossRef](#)]
30. Olimstad, G.; Nielsen, T.; Børresen, B. Dependency on runner geometry for reversible-pump turbine characteristics in turbine mode of operation. *J. Fluids Eng.* **2012**, *134*, 121102. [[CrossRef](#)]

Disclaimer/Publisher’s Note: The statements, opinions and data contained in all publications are solely those of the individual author(s) and contributor(s) and not of MDPI and/or the editor(s). MDPI and/or the editor(s) disclaim responsibility for any injury to people or property resulting from any ideas, methods, instructions or products referred to in the content.